Relationship Between Capacity and Pathloss for Indoor MIMO Channels

Nielsen, Jesper Ødum; Andersen, Jørgen Bach; Bauch, Gerhard; Herdin, Markus

Published in:
IEEE 17th International Symposium on Personal, Indoor and Mobile Radio Communications, 2006

DOI (link to publication from Publisher):
10.1109/PIMRC.2006.253925

Publication date:
2006

Document Version
Publisher's PDF, also known as Version of record

The 17th Annual IEEE International Symposium on Personal, Indoor and Mobile Radio Communications (PIMRC'06)

RELATIONSHIP BETWEEN CAPACITY AND PATHLOSS FOR INDOOR MIMO CHANNELS

Jesper Ødum Nielsen, Jørgen Bach Andersen

Department of Communication Technology
Aalborg University
Niels Jernes Vej 12, 9220 Aalborg, Denmark
{jni,jba}@kom.aau.dk

Gerhard Bauch, Markus Herdin

DoCoMo Euro-Labs
Landsbergerstraße 312, 80687 Munich, Germany
{bauch,herdin}@docomolab-euro.com

ABSTRACT

MIMO transmission systems exploit scattering in the radio channel to achieve high capacity for a given SNR. A high pathloss is generally expected for channels with rich scattering, suggesting that a high SNR and rich multipath are competing goals. The current work investigates this issue based on measurements obtained with a 16×32 MIMO channel sounder for the 5.8 GHz band. The measurements were carried out in various indoor scenarios where different sizes of both the transmitter and receiver antenna arrays are investigated, 1×1 up to 16×32. A moderate correlation between pathloss and median capacity was found. However, the higher richness can not compensate for the decrease in capacity due to increased pathloss. Assuming a fixed Tx power, the median capacity was found to depend approximately linearly on the pathloss. The slope of the linear relation depends on the effective rank of the channel, which in turn was found to be approximately linearly dependent on the number of antennas, assuming a symmetric MIMO channel.

I INTRODUCTION

Future wireless communications devices are expected to offer bit rates of several hundred Mbit/s. This will require high spectral efficiencies of the transmission systems because the radio spectrum available for each pair of transceivers is limited. Systems using multiple-input multiple-output (MIMO) transmission techniques are promising in this aspect and have been studied intensely recently [1, 2]. However, the capacity of MIMO systems is highly dependent on the mobile channel properties [3, 4].

The focus of this work is MIMO transmission for mobile devices in an indoor environment where a large capacity is expected because of a generally high degree of signal scattering and lack of line of sight (LOS) in many cases. MIMO systems benefit from channels with a high degree of scattering since this increases the rank of the channel. However, the capacity is also highly dependent on the channel signal to noise ratio (SNR), and a high SNR may imply a low degree of scattering, as reported in [5]. Hence, it may be a question of which effect is dominating. The current paper reports on results obtained from measurements with a wideband 16×32 MIMO channel sounder for the 5.8 GHz band. The measurements were carried out in widely different indoor environments and includes both temporal and spatial aspects of channel changes. The capacities of the observed channels are studied and compared with pathloss, and the capacity of fixed transmit power systems is investigated.

II MEASUREMENTS

The measured data used in the current work is obtained using a MIMO channel sounder operating at a carrier frequency of 5.8 GHz. The sounder uses the correlation principle, and measures 16 transmit channels simultaneously, where each transmit branch uses a 1 W power amplifier. On the receive side four channels were measured in parallel, and using switching each branch is extended so that in total 32 receive channels are measured. Additional information about the sounder is available in [6]. The full complex 16×32 MIMO channel is measured in a time-triggered way at a rate of 60 Hz. In a post-processing procedure the measurements are compensated for the sounder system response and the bandwidth is limited to about 100 MHz.

All measurements were made using planar arrays of monopole antenna elements arranged in rectangular grids with a spacing of 2.5 cm, or 0.48λ. For the transmitter array the active elements are arranged in a 4×4 grid while the receiver array is 4×8.

During measurements the transmitter array is moved along a horizontal half-circular path with a radius of about 0.5 m. The speed along the arc is about 52 mm/s or about one λ/s. The transmitter array and the device for movement is depicted in Fig. 1. The distance from the array ground plane to the floor is about 90 cm.

Simultaneously with the transmitter array movements, the receiver array is moved linearly while the measurements take place, at a speed of about 30 mm/s corresponding to about 0.6λ/s. The distance from the array ground plane to the floor is 94 cm.

All the measurements were made within the same modern four story (including basement) office building. The building is primarily made of reinforced concrete with an outer brick wall and with most inner partitions made in light plaster board construction. The floors/ceilings of each level are also made of concrete. The measurement campaign was divided into a number of different scenarios, described in the following subsections.

A *Open Lab*

In this scenario both transceivers are located inside or nearby a large room, containing much furniture and equipment, including bookshelves and room partitioning that may block the LOS

1-4244-0330-8/06/$20.00

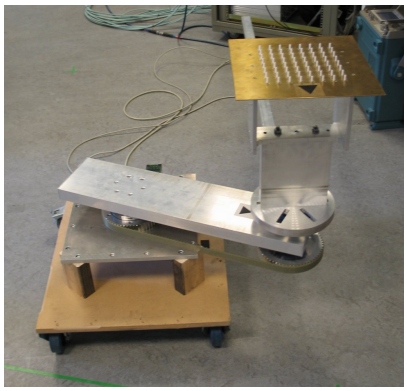

Figure 1: The pedestal for circular movement of the transmitter array including the 4×4 planar array of monopole elements with dummy elements. The element spacing is 2.5 cm.

between the transmitter (Tx) and receiver (Rx). In addition people activity can be expected in this room. For all of these measurements the Tx array was located in the corridor next to the open lab environment, but LOS was blocked in all cases. The main part of the lab has dimensions of about 13 m$\times$ 7 m, see Fig. 2 where the floor plan of the 2nd floor is shown. The Tx was located at the place indicated by 'T_{lab}' on the drawing. The different Rx locations are also shown on the floor plan, labelled 'L1' to 'L5'.

B *Office to Office*

In this scenario both the Tx and Rx arrays are located inside small offices next to the 2nd floor corridor. The Tx location is labelled 'T_{off}' in Fig. 2 while the Rx locations are 'O1', 'O2', and 'O3'.

C *Building Level Crossing*

For these measurements the Tx array is on the 1st floor and the Rx is on the 2nd floor. In this situation most of the energy can be expected to propagate via corridors and staircases. The two floors are connected to a main entrance hall which covers the full height of the building. The Tx array is in the location labelled 'T_{Lvl}', which is indicated on the 2nd floor plan shown in Fig. 2, but in reality is on the 1st floor.

The measurements of this scenario are labelled V1, V2, and V3, corresponding to the Rx array locations, shown on the floor plan.

D *Basement*

In this case both the Tx and the Rx are located inside the same large room on the basement floor. This is a storage room which has concrete floor, ceiling and walls where the ceiling is cluttered with various pipes, lamps, *etc.* The room joins a corridor in one side. For the measurements selected for the current work the Tx is located in one corner of the room (south-east) and the Rx in the corridor opposite the room at three different positions. For the 'B1' measurement the Rx at south-west, near

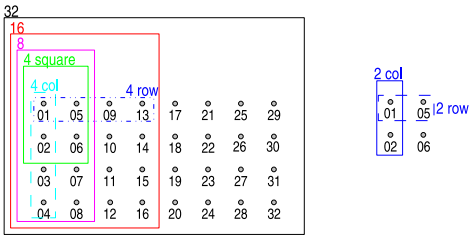

Figure 3: Sub-array selections. The frames indicate which array elements are included at each end. For clarity the selection of two elements are shown seperately on the right.

non-line of sight (NLOS) condition. The Rx is in LOS condition in the 'B2' measurement west of the Tx, and finally for the 'B5' measurement the Rx is in the corridor north of the room, NLOS condition.

In addition to the channel changes introduced by the movements of the transceivers, other changes in the channel can also be expected since the measurements were carried out while normal work activity took place in the building.

III Results

For each of the environments mentioned above, such as L1, O3, and B2, a series of MIMO channel measurements were made at a 60 Hz rate while both the Tx and Rx arrays were moving. In the following the first 600 MIMO channel measurements of each measurement series are used for analysis, corresponding to 10 s or about 10 wavelengths of movement in space for the Tx array. This distance was assumed to be sufficiently short to justify an assumption of a stationary channel and long enough to allow for a proper averaging. The stationarity issue is discussed further in [6], based on the same set of measurements.

Although the measurements are wideband all results in the current paper are derived from narrowband data. Before computing capacity the power of each $\mathbf{H}$ matrix in a measured series was normalized, where the power was estimated for each $\mathbf{H}$ matrix as the average over all 16×32 Tx and Rx antenna combinations, corresponding to averaging in space.

Data arising from sub-sets of the arrays used during the measurements are used to estimate the performance of smaller arrays. The sub-arrays are denoted as $Tx \times Rx$ where Tx and Rx are subsets as shown in Fig. 3. Note that the selection of 32 elements is only possible at the Rx.

For the narrowband channel the received signal can be described as $\mathbf{y} = \mathbf{Hs} + \mathbf{n}$, where $\mathbf{s}$ is the vector of transmitted symbols with length M, $\mathbf{n}$ is a same size noise vector, and $\mathbf{H}$ is the $N \times M$ random channel matrix. Assuming that the transmitter has no knowledge of the channel, the capacity of the channel is given by [2]

$$C = \sum_{i=1}^{I} \log_2 \left(1 + \frac{\rho}{M} \lambda_i\right) \tag{1}$$

where ρ is the SNR, $I = \min\{M,N\}$ and λ_i is the i'th eigenvalue of the matrix $\mathbf{HH}^H$. Since it is dependent on the random

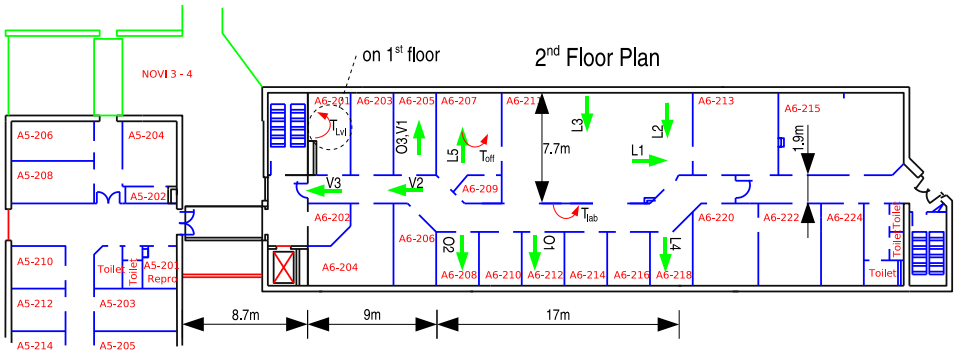

Figure 2: Overview of measurement site and transceiver locations on the 2nd floor.

channel matrix **H**, the capacity is a random variable and must be characterized in statistical terms. For the measurements described in Section II this was done in [6] where cumulative distribution functions (CDFs) were obtained and compared to CDFs for model data. As in other similar works this analysis was carried out using normalized **H** matrices and hence the pathloss of the channel was removed from the measurements, as described above. This is analogous to assuming a perfect power control in the MIMO system.

As given by (1) the capacity of a MIMO system depends on both the channel eigenvalues and on the SNR. From the viewpoint of ensuring a minimum channel capacity one might hope that a decrease in SNR due to increased pathloss could be compensated by an increased richness in the channel. In order to investigate whether this is the case for the present measurements, both the median capacity and the pathloss were computed for each measurement, where the pathloss is computed using the total power gain averaged over all instantaneous measurement locations, transmitter and receiver elements. Fig. 4 shows scatter plots of the median measured capacity versus the pathloss for all measurements, where the plots in the figure represent the 16×32, 8×8, and 2×2 column antenna array constellations, respectively. The capacities are computed for an SNR of 10 dB for all the locations, irrespective of the pathloss.

From the scatter plots some correlation seems to be present at least for the large arrays, although much of the apparent correlation can be attributed to the data for the B2 and O3 environments. Table 1 lists the estimated correlation coefficents for all of the array configurations, confirming the impression of a moderate correlation.

In the results discussed above the SNR is kept constant at 10 dB meaning that the transmitted power must be lowest for the lowest pathloss, and hence extra capacity will be available if the received power is allowed to increase to the level the system is able to deliver. In the following the dependence of the capacity on the pathloss is considered in a system that has a fixed Tx power resulting in an SNR of 15 dB at a pathloss of about 86 dB, corresponding to halfway between the minimum and maximum measured pathloss. This was done by computing the capacity of the different environments for SNRs of $0, 5, \ldots, 30$ dB, and the fixed Tx power capacity was then

Table 1: Correlation coefficient of pathloss and median capacity.

Array constellation	Correlation coeff.
16×32	0.6
16×16	0.6
8×8	0.7
4×4 col	0.3
4×4 row	0.6
4×4 col/row	0.4
4×4 row/col	0.7
4×4 square	0.7
2×2 col	0.2
2×2 col/row	0.4
2×2 row/col	0.4
2×2 row	0.3
1×1	0.0

obtained as the capacity at the adjusted SNR, via interpolation, according to the pathloss compared to the reference pathloss. The maximum SNR was limited to 30 dB in order to prevent noise in the measurements to appear as channel richness.

In Fig. 5 the results for the 16×32 and 4×4 row/colmn array constellations are shown, where the red circles indicate the measured points and the red lines are lest-squares linear fits to the data. It is noted that the measured data are obtained for different Rx and Tx locations, as explained in Section II. Also note that the O3, B5, and V2 environments are excluded since the pathloss is such that the resulting SNR is below 0 dB or above 30 dB.

From the figure a near linear dependence of the median capacity and the pathloss is clear, at least within the about 25 dB pathloss range observed. Similar observations are made for all the other array constellations (not shown).

It is interesting to compare these findings with those reported in [7]. In this work the capacity of different measured channels, including pathloss, could be obtained approximately, by varying the SNR for a single measurement. Hence, it was concluded that the pathloss was dominant in determining the mean capacity whereas the channel richness is less important and the influence approximately the same for all the measure-

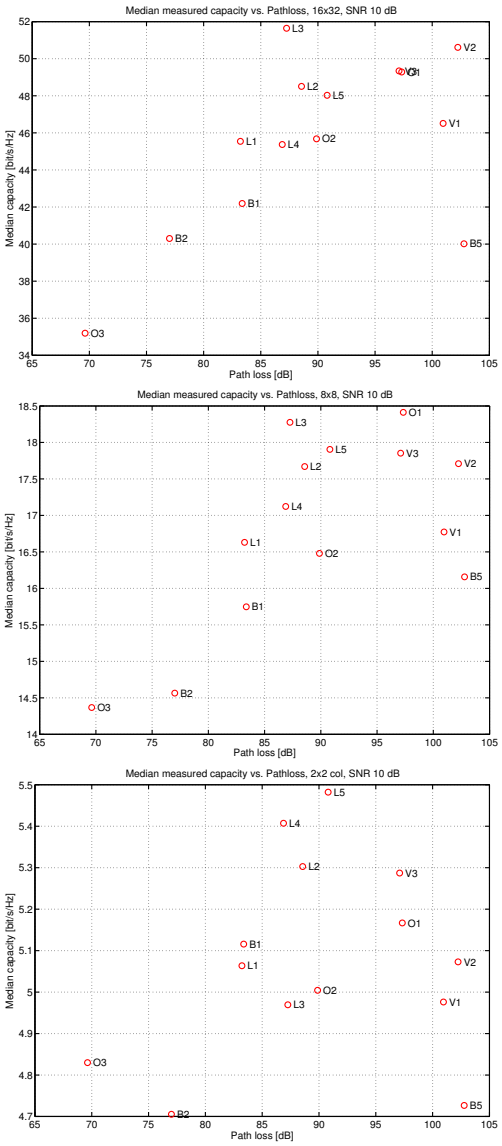

Figure 4: Measured median channel capacity versus pathloss for different locations and for array constellations (Tx $\times$ Rx), 16×32 (top), 8×8 (middle), 2×2, column (bottom). The capacity is for an SNR of 10 dB.

ments. As opposed to the findings of the current work, however, the mean capacity was not found the be linearly related to the pathloss. It should be noted that the results in [7] are obtained from measurements in a seemingly relatively homogeneous measurement environment, in a static channel and using an 8×8 MIMO system. In comparison, the measurements of the current work involves quite different types of measurement scenarios and includes channel changes during the measurements.

Using a Taylor series the capacity in (1) may be written as

$$C = \sum_{i=1}^{I} \log_2\left(\frac{\rho\lambda_i}{M}\right) - \sum_{n=1}^{\infty} \frac{(-1)^n}{n\log_e(2)} \left(\frac{M}{\rho\lambda_i}\right)^n \tag{2}$$

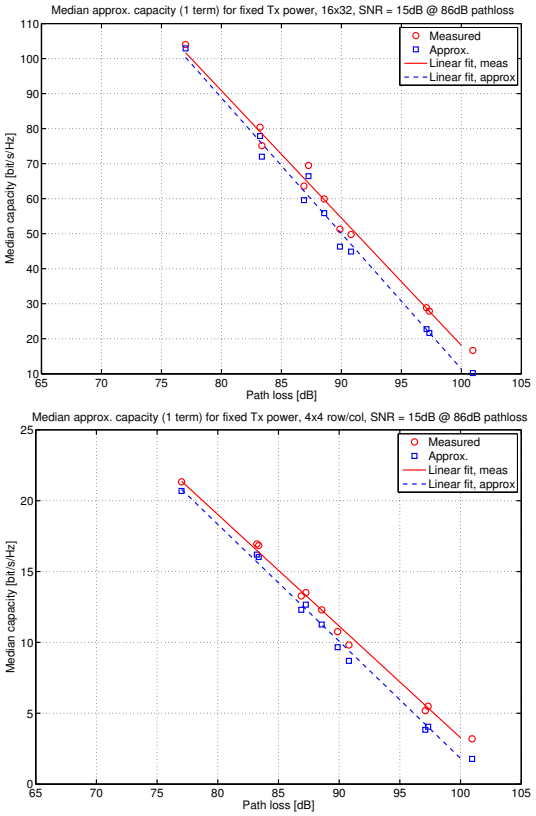

Figure 5: Median channel capacity versus pathloss for fixed Tx power and array constellation (Tx $\times$ Rx) 16×32 (top), and 4×4, row/column (bottom). Results are shown as points for both actual and approximate capacity, and also best linear fits are shown as lines.

where the series converges on the condition that $r_i = M/(\rho\lambda_i) < 1$. The contribution of the eigenvalues for which $r_i \geq 1$ to (1) are $\log_2(1+1/r_i) \leq 1$ and hence in many cases will be insignificant compared to the terms for which $r_i < 1$. Simply omitting the terms (2) may be rewritten as

$$C \simeq \frac{\log_2(10)}{10} \cdot J(\rho)\rho_{\text{dB}} \tag{3a}$$

$$+ \sum_{i=1}^{J(\rho)} \log_2(\lambda_i) - J(\rho)\log_2(M) \tag{3b}$$

$$- \sum_{i=1}^{J(\rho)} \sum_{n=1}^{\infty} \frac{(-1)^n}{n\log_e(2)} \left(\frac{M}{\rho\lambda_i}\right)^n \tag{3c}$$

where ρ_{dB} is the SNR in dB and $J(\rho)$ is the *effective channel rank* defined as the maximum i such that $M < \rho\lambda_i$, assuming the eigenvalues are sorted in decreasing order. It can be noted that for large SNR the terms in (3c) vanishes, $J = I$, and the approximation is identical to the one given in [8], where the first term of (3b) is defined as the channel *richness*. Below the term *effective richness* is used since it here depends on J.

In order to assess how close the approximation is in practice the capacity of the measured data was computed using (3) and shown in Fig. 5 as the blue squares. Also linear fits were com-

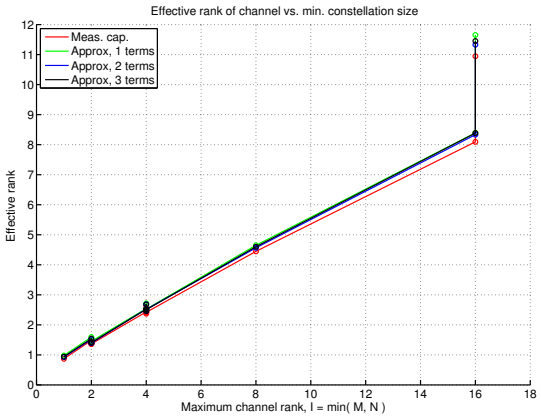

Figure 6: The effective rank, J, versus maximum channel rank, $I = \min(M,N)$. The rank is obtained from linear fits to the measured capacity as well as the capacity approximated using 1–3 terms.

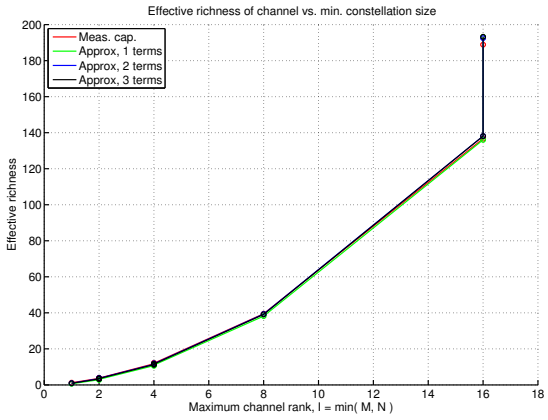

Figure 7: The effective channel richness versus maximum channel rank, $I = \min(M,N)$. The richness is obtained from linear fits to the measured capacity as well as the capacity approximated using 1–3 terms.

puted, shown with the blue dashed lines. The approximations are computed using only the linear parts of (3), *i.e.*, omitting the term (3c), which in practice only improves the approximations marginally. From the plots it appears that the approximations are quite close and the general linear dependence on the SNR is retained, although the slope is slightly larger, since the approximation gets worse with lower SNR.

Although the channels with a high pathloss may have higher richness compared to low pathloss channels, as the results of Table 1 might indicate, the linear relation shows that the SNR is the most important.

The linear relation is found for all the array constellations, but the parameters, the slope and additive constant, depend on the number of elements. According to (3) the slope is $J\log_2(10)/10 \simeq J \cdot 0.33$ and hence the effective rank is easily found from the slope of the linear fits, such as in Fig. 5. The effective ranks for the different array constellations are shown in Fig. 6, where it is noticed that for the symmetric constellations ($M = N$) the rank grows roughly linearly as $J \simeq 0.5 \cdot I$. As expected, for the 16×32 constellation J is larger than for 16×16. Finally, it is noticed that the J-values obtained from the approximated capacities are close to those obtained from the measured capacities. The effective channel richness versus the maximum channel rank is shown in Fig. 7.

IV Conclusion

The current work investigates relations between the pathloss and the median channel capacity for indoor MIMO channels. The investigation is based on channel measurements in widely different indoor scenarios, using arrays with 16 Tx and 32 Rx elements. A moderate positive correlation between pathloss and the median capacity was found for a fixed SNR, so that to some degree the channel richness compensates for the decrease in median capacity due to extra pathloss. However, for fixed transmit power the median capacity generally decreases with increasing pathloss. The decrease was found to be approximately linearly related to the pathloss, with parameters depending on the array constellation. For the symmetric Tx and Rx array constellations the median capacity decreases with approximately $0.17 \cdot I$ bit/s/Hz/dB, where I is the number of antenna elements at each side.

References

[1] G. Foschini and M. J. Gans, "On limits of wireless communications in a fading environment when using multiple antennas," *Wireless Personal Communications*, vol. 6, no. 3, pp. 311–335, Mar. 1998.

[2] D. Gesbert, M. Shafi, D. shan Shiu, P. J. Smith, and A. Naguib, "From theory to practice: An overview of MIMO space-time coded wireless systems," *IEEE Journal on Selected Areas in Communications*, vol. 21, no. 3, pp. 281–302, Apr. 2003.

[3] M. Herdin, H. Özcelik, H. Hofstetter, and E. Bonek, "Variation of measured indoor MIMO capacity with receive direction and position at 5.2 GHz," *Electronics Letters*, vol. 38, no. 21, pp. 1283–1285, Oct. 2002.

[4] J. Wallace, M. Jensen, A. Swindlehurst, and B. Jeffs, "Experimental characterization of the MIMO wireless channel: data acquisition and analysis," *IEEE Transactions on Wireless Communications*, vol. 2, no. 2, pp. 335–375, Mar. 2003.

[5] T. Svantesson and J. Wallace, "On signal strength and multipath richness in multi-input multi-output systems," in *Proceedings of IEEE International Conference on Communications (ICC'03).*, vol. 4, 2003, pp. 2683–2687.

[6] J. Ø. Nielsen and J. B. Andersen, "Indoor MIMO channel measurement and modeling," in *The Proceedings of the International Symposium on Wireless Personal Multimedia Communications (WPMC'05)*, 2005, pp. 479–483.

[7] H. Özcelik, M. Herdin, R. Prestros, and E. Bonek, "How MIMO capacity is linked with single element fading statistics," in *International Conference on Electromagnetics in Advanced Applications (ICEAA)*, 2003, pp. 775–778.

[8] J. B. Andersen and J. Ø. Nielsen, "Modelling the full MIMO matrix using the richness function," in *Proceedings of the ITG/IEEE Workshop on Smart Antennas (WSA) 2005*, Apr. 2005.